Biosensors and Bioelectronics 212 (2022) 114407

Contents lists available at ScienceDirect

Biosensors and Bioelectronics

journal homepage: www.elsevier.com/locate/bios

Cell-mimetic biosensors to detect avian influenza virus via viral fusion

Geunseon Park [a], Jong-Woo Lim [b], Chaewon Park [a], Minjoo Yeom [b], Sojeong Lee [a], Kwang-Soo Lyoo [c], Daesub Song [b,**], Seungjoo Haam [a,*]

[a] Department of Chemical and Biomolecular Engineering, Yonsei University, Seoul, 03722, Republic of Korea
[b] Department of Veterinary Medicine Virology Laboratory, College of Veterinary Medicine and Research Institute for Veterinary Science, Seoul National University, Seoul, 08826, Republic of Korea
[c] College of Veterinary Medicine, Jeonbuk National University, Iksan, 54596, Republic of Korea

ARTICLE INFO

Keywords:
Avian influenza
Pathogenicity
Viral fusion
Enzymatic activation
Cell-mimetic nanostructure
Biosensor

ABSTRACT

Avian influenza virus (AIV) causes acute infectious diseases in poultry, critically impacting food supply. Highly pathogenic avian influenza viruses (HPAIVs), in particular, cause morbidity and mortality, resulting in significant economic losses in the poultry industry. To prevent the spread of HPAIVs, detection at early stages is critical to implement effective countermeasures such as quarantine and isolation. Through a viral fusion mechanism, cell-mimetic nanoparticles (CMPs), developed in the current study, can rapidly detect HPAIV and low pathogenic AIV (LPAIV). The CMPs comprise polymeric nanoparticles, which are constructed using sialic acid and fluorescence resonance energy transfer (FRET) dye pairs that expose the FRET off signal in response to LPAIV and HPAIV, after activation by enzymatic cleavage in the endosomal environment. The CMPs detect a wide variety of LPAIVs and HPAIVs in biological environments. Additionally, the cross-reactivity of CMPs is determined by testing their function with different viral species. Therefore, these findings demonstrate the significant potential of the proposed strategy for mimicking viral infection in vitro and using them as a highly effective diagnostic assay to rapidly detect LPAIV and HPAIV, preventing economic losses associated with viral outbreaks.

1. Introduction

Avian influenza virus (AIV) causes acute infectious diseases in poultry such as chickens, ducks, and turkeys, resulting in significant economic losses. AIVs are further classified into highly pathogenic avian influenza virus (HPAIV) or low pathogenic avian influenza virus (LPAIV), with HPAIV designated as a disease requiring management by the World Organisation for Animal Health (OIE) due to high risk of infection (Fukuyama et al., 2015; Kittel et al., 2004; Manicassamy et al., 2010). Since HPAIV spreads rapidly to the host and causes extremely high rates of morbidity and mortality, it is critical to distinguish HPAIV to accord preventive measures, such as quarantine and isolation, to minimize economic losses.

Various diagnostic methods have been used to detect AIV. Rapid test kits based on antigen-antibody reactions are widely used because of their ease of use and on-the-spot analysis. While these kits are capable of rapidly detecting AIV, their low sensitivity and poor specificity present significant concerns. Additionally, conventional approaches, such as enzyme-linked immunosorbent assays (ELISA), are time-consuming and offer low sensitivity. Moreover, conventional assays are incapable of discriminating HPAIV from LPAIV and thus contribute only a limited amount to the preventive measures against AIV pathogenicity. Reverse transcription polymerase chain reaction (RT-PCR) is the gold standard diagnostic method for the precise analysis of a wide variety of pathogens. Although RT-PCR is a sensitive and accurate method for detecting AIV by amplifying viral nucleic acids extracted from virus samples, the diagnostic assay requires a significant amount of time, professional skill, and laboratory setup, inevitably limiting accessibility of on-site detection (Hennechart-Collette et al., 2014; Nyan and Swinson, 2015; Tsang et al., 2016; Ye et al., 2014). To overcome the limitations of existing diagnostic assays, the physiological properties of viruses have been prioritized in the development of advanced biosensors.

AIV uniquely infects host cells via specific binding of viral proteins to the cellular receptor for sialic acid (SA) (Imai et al., 2012; Neumann et al., 2009; Stech et al., 2005). Thus, AIV can adhere to host cells efficiently due to receptor-mediated binding. Under acidic conditions,

* Corresponding author.
** Corresponding author.
E-mail addresses: sds@snu.ac.kr (D. Song), haam@yonsei.ac.kr (S. Haam).

https://doi.org/10.1016/j.bios.2022.114407
Received 4 April 2022; Received in revised form 6 May 2022; Accepted 17 May 2022
Available online 20 May 2022

AIV can penetrate the cellular membrane via fusion peptides derived from the viral protein hemagglutinin (HA).

Proactive expression of the fusion peptide requires a conformational change in HA, which is induced by proteolytic cleavage by trypsin- or furin-like proteases (Wang et al., 2016; Yassine et al., 2015; Yoon et al., 2015). Additionally, LPAIVs have monobasic cleavage sites with a single arginine (-R-) that are typically activated by a trypsin-like enzyme. As a result, LPAIV infection is restricted to the respiratory and intestinal tracts, which express trypsin-like proteases, resulting in mild infection. However, because HPAIVs contain multiple basic sites such as R/K-R-K-K (where K represents lysine), they can be activated by both trypsin- and furin-like proteases (Collins et al., 2019; Höfle et al., 2012). Additionally, HPAIVs can progress to severe systemic infections because furin is a ubiquitously expressed protease in the host (Lee et al., 2015; Welch et al., 2013). Because the tissue tropism of AIV is a critical determinant of virulence, the difference in the proteases required for viral infection between LPAIV and HPAIV can serve as a rational basis for detecting AIVs and further discriminating HPAIV from LPAIV (Galloway et al., 2013; Lee et al., 2016). The current study reports the development of cell-mimetic nanoparticles (CMPs) for rapidly detecting HPAIV and LPAIV by exploiting the fusogenic behavior of HA under enzymatic activation (Scheme 1). The CMPs were synthesized using polymeric nanoparticles (NPs) containing fluorescence resonance energy transfer (FRET) pair fluorophores and SA incorporated into the particles to facilitate interaction with AIV (Barrabés et al., 2010; Chen et al., 2018; Kim et al. 2013, 2017; Wagner et al., 2013; Xiao et al., 2010). The fusion peptide of the virus, expressed in the endosomes, efficiently penetrates and fuses with the membrane of the CMPs via HA-SA binding. Furthermore, membrane fusion events alter the efficiency of the FRET pairs, generating optical signals and enabling the detection of AIV with high sensitivity. Lastly, the disparity in the proteolytic cleavage of HA between LPAIV and HPAIV was used to further differentiate LPAIV and HPAIV. The proposed strategy of utilizing viral infection with AIV via a cell-mimetic biosensor offers a user-friendly and rapid approach to detect HPAIV and LPAIV with high sensitivity and specificity.

2. Experimental section

2.1. Materials

Methoxy-poly(ethylene glycol) (mPEG) with a molecular weight of 2 kDa, D,L-lactide (3,6-dimethyl-1,4-dioxane-2,5-dione), stannous octoate ($Sn(Oct)_2$), chloroform-d, trypsin from bovine pancreas, sodium acetate buffer solution (pH 5.2), phosphotungstic acid, and Triton X-100 were obtained from Sigma-Aldrich (St. Louis, USA). Diethyl ether, chloroform, n-hexane, and toluene were obtained from DUKSAN (Ansan, Republic of Korea). 3,3′-Dioctadecyloxacarbocyanine perchlorate (DiO) and 1,1′-dioctadecyl-3,3,3′,3′-tetramethylindocarbocyanine perchlorate (DiI) were purchased from Thermo Fisher Scientific (Waltham, USA). All other chemicals and reagents used were of analytical grade. Formvar 400-mesh copper grids were purchased from Ted Pella, Inc. (Redding, USA).

2.2. Synthesis of mPEG-b-PLA

Methoxy-poly(ethylene glycol)-block-poly lactic acid (mPEG-b-PLA) was synthesized via ring-opening polymerization of D,L-lactide using hydroxyl-terminated mPEG as the initiator and $Sn(Oct)_2$ as the catalyst.[44, 45] A three-necked flask was filled with mPEG dissolved in

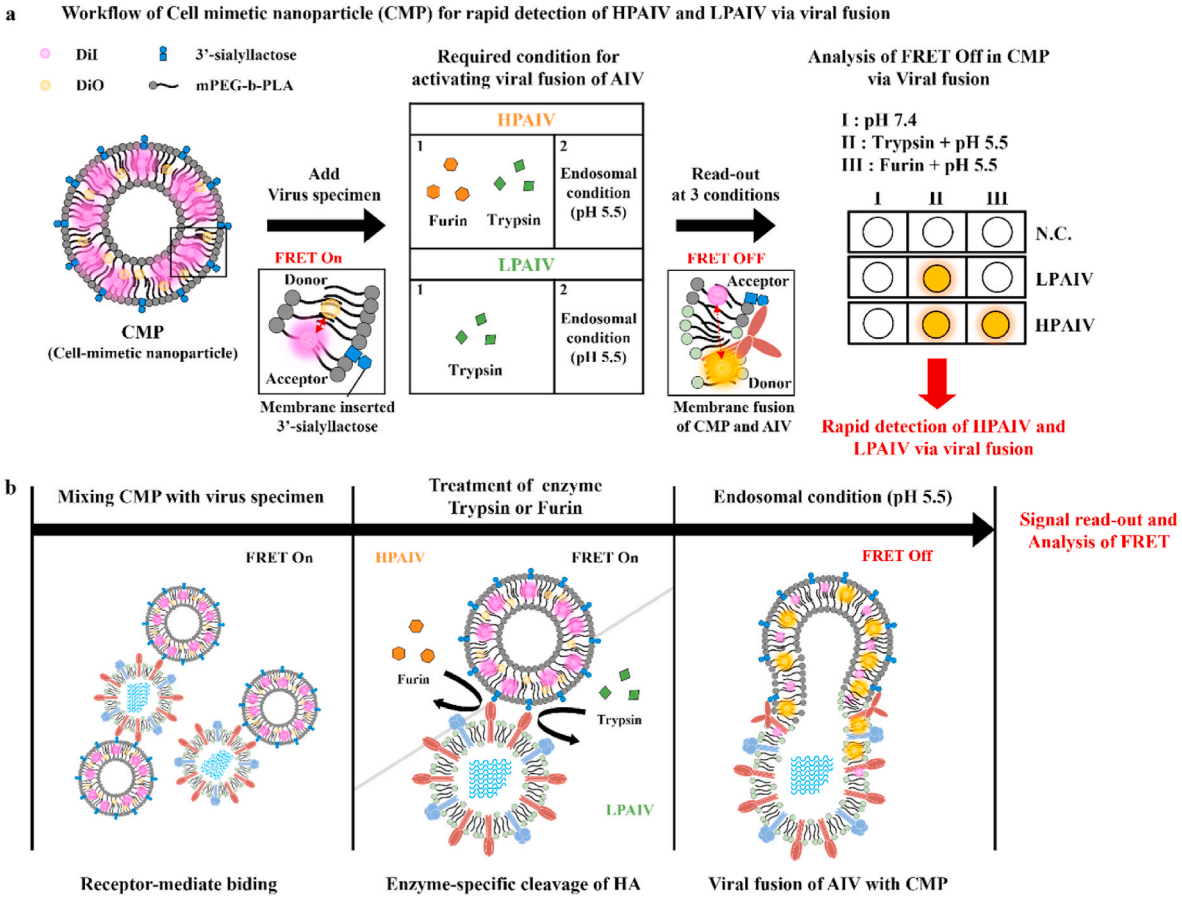

Scheme 1. Schematic illustration of a) the workflow of a cell-mimetic nanoparticle (CMP) for the rapid detection of HPAIV and LPAIV via viral fusion; b) mechanism of CMP exhibiting receptor-mediated binding and membrane fusion with AIV, activated by the enzyme-specific cleavage of HA and endosomal condition (pH 5.5).

toluene. Various concentrations of D,L-lactide and $Sn(Oct)_2$ (0.05 wt% mPEG and D,L-lactide) were added dropwise to the flask, and the reaction mixture was heated under reflux at 120 °C overnight under a nitrogen atmosphere. After completion of the reaction, the residual solvent in the resulting solution was removed using a rotary evaporator. The product was filtered using a Buchner funnel and vacuum-dried for at least one day at room temperature. Proton (^1H) NMR spectroscopy was used to determine the molecular weight and f-value of the synthesized mPEG-b-PLA (400 MHz NMR spectrometer, Bruker, Germany). To confirm the polymerization process, the polymer was dispensed in chloroform-d ($CDCl_3$) and loaded onto a 400 MHz ^1H NMR spectrometer. To analyze the chemical structure, the characteristic peaks of the polymer were integrated. Chemical shifts are shown in ppm on the δ scale. ^1H NMR (400 MHz, $CDCl_3$) δ: 3.65 (–CH_2– of PLA), 3.38 (–OCH_3– of mPEG).

2.3. Preparation of cell-mimetic nanoparticles (CMPs)

To fabricate cell-mimetic nanoparticles, mPEG-b-PLA with a range of f-values was used. mPEG-b-PLA and the FRET dye pair DiO and DiI were dissolved in 1 mL of chloroform at a molar ratio of 74.7:1.1:1, in a round-bottom flask and then completely dried to remove any remaining organic solvents. The dried mixture was hydrated in a buffer containing 20 mM 4-(2-hydroxyethyl)-1-piperazineethanesulfonic acid [HEPES], 0.1 M KCl, and 0.5% N-octyl-β-D-glucopyranoside (OG). The ratio of 3′-sialyllactose to the hydrated film was 2:1. Following a 12-h incubation at 50 °C with stirring, the mixture was rapidly diluted four-fold to bring the OG concentration below the critical micelle concentration. This diluted mixture was dialyzed for three days at room temperature in 2 L of the same buffer. Dynamic laser scattering (ELSZ, Otsuka Electronics, Osaka, Japan) was used to determine the size distribution of CMP and nanoparticles without insertion (NP). CMP was negatively stained with phosphotungstic acid (PTA), and images were captured using transmission electron microscopy (TEM) (JEM-F200, JEOL, Tokyo, Japan).

2.4. Fluorescence spectra analysis

The fluorescence spectra of CMP was analyzed using a multimode microplate reader (SpectraMax i3x, Molecular Devices, San Jose, USA) with emission wavelengths ranging from 504 to 599 nm and an excitation wavelength of 475 nm. To determine the proportion of the FRET effect in this study, the FRET efficiency of CMP was determined using the fluorescence intensities (FIs) of DiO and DiI as a donor and acceptor, respectively (**Equation (1)**). We used FEC (%) as a parameter to describe the capacity of CMP to respond to a sample, demonstrating that FRET efficiency decreased significantly when CMP was disrupted with Triton X-100 (TX-100), whereas a saturated FRET efficiency was obtained in DW (**Equation (2)**).

$$FRET\ Efficiency = (FI_{DiI}) / (FI_{DiO} + FI_{DiI}) \quad \text{(Equation 1)}$$

$$FRET\ Efficiency\ change\ (FEC) = \frac{(E_{dw} - E_{sample})}{(E_{dw} - E_{TX-100})} \times 100 \quad \text{(Equation 2)}$$

2.5. Preparation of virus samples

LPAIVs (H1N1, H2N5, H3N1, H4N6, H5N2, H6N8, H7N7, H9N2, H9N10, H10N7, and H11N9), two HPAIVs (H5N1 and H5N6), and Newcastle disease virus (NDV) were propagated in the allantoic cavity of 11-day-old embryonated chicken eggs. Each virus stock (100 μL) was inoculated into the allantoic cavity of the chicken eggs. Porcine epidemic diarrhea virus (PEDV) and canine distemper virus (CDV) were propagated in Vero cells, and porcine reproductive and respiratory syndrome virus (PRRSV) and infectious canine hepatitis virus (ICHV) were propagated in MARC-145 and MDCK cells, respectively. After a 72-h incubation at 37 °C, the culture medium was chilled overnight at 4 °C. Subsequently, the media containing the propagated viruses were harvested and purified by centrifugation at 4000 rpm for 20 min. The supernatant was immediately frozen at −80 °C for long-term storage and future use in the assay.

Two types of feces were used to prepare fecal viral samples: chicken and duck feces. LPAIVs and HPAIVs were combined with negative feces at a volume ratio of 1:10 and allowed to stand for 1 h. A swab and syringe were used to filter and collect aqueous fecal samples in accordance with the rapid kit detection process.

2.6. Biosafety

All experimental procedures, including preparation of samples associated with HPAIV specimens, were performed in an animal biosafety level III (ABSL3) facility at the Korea Zoonosis Research Institute (KOZRI) at the Jeonbuk National University.

2.7. Virus detection method

The virus detection procedure involved preincubation of viral specimens (25 μL) and 50 μL CMP (1 mg mL^{-1}) for 40 min with 25 μL trypsin (0.1 mg mL^{-1}) or furin (1:1000 diluted unit). The mixture was then incubated for an additional 20 min in 25 μL of 300 mM sodium acetate buffer (pH 5.2). The fluorescence spectrum was monitored using a multimode microplate reader from 504 nm to 599 nm in 5 nm steps (SpectraMax i3x, Molecular Devices).

3. Results and discussion

3.1. Preparation and characterization of cell-mimetic nanoparticle (CMP)

To achieve fusogenic interaction with AIV, CMPs were designed to exhibit key characteristics of cell membranes, including a bilayer structure containing cellular receptors such as sialic acid, an AIV-binding moiety. The CMPs were constructed via a thin-film hydration method using amphiphilic Methoxy-poly(ethylene glycol)-block-poly lactic acid (mPEG-b-PLA) (Peterson et al., 2015; Zhu, 2013). mPEG-b-PLA was synthesized by ring-opening polymerization, and nuclear magnetic resonance (NMR) was used to determine the chemical structure and molecular weight of the synthesized copolymer (Fig. S1 (a))

The polymer film was formed by evaporating chloroform and hydrating it with a reaction buffer containing N-octyl-β-D-glucopyranoside (OG) and sialic acid. To take advantage of the receptor specificity of AIV for sialic acid linked to galactose (Gal) via an alpha 2, 3 linkage (SA alpha 2,3-Gal), 3′-sialyllactose was used. To prepare the bilayer vesicle nanostructure containing sialic acid, the hydrated film was sonicated using a tip sonicator and purified by dialysis against the reaction buffer. Dynamic light scattering (DLS) (Fig. 1(a)) and transmission electron microscopy (TEM) (Fig. 1(c)) were used to determine the size and morphology of the CMP, respectively. The average diameter of the CMPs was 100 nm, and the TEM image revealed a bilayer structure consisting of a hydrophilic interior and hydrophobic shell of PLA. Through hydrophobic interactions, the cell-like CMP efficiently encapsulated FRET pair dyes (donor dye, DiO and acceptor dye, DiI) in the shell region. Zeta potential analysis confirmed the presence of a negative charge on the surface of the CMPs, which was similar to the surface charge of the sialic acid-rich region of the cellular membrane (Fig. 1(b)). To assess sialic acid incorporation into the membrane structure, the CMPs were qualitatively analyzed using Fourier-transform infrared spectroscopy (FT-IR), and the presence of specific peaks of sialic acid, including the asymmetric stretching vibration of carboxylate (COO-) at 1605 cm^{-1} and N–H bend at 1550 cm^{-1}, was confirmed (Fig. S1(b)). Characteristic peaks at 1750 cm^{-1} can be assigned to carbonyl stretching (C=O) of the ester in mPEG-b-PLA, representing successful incorporation of sialic acid and

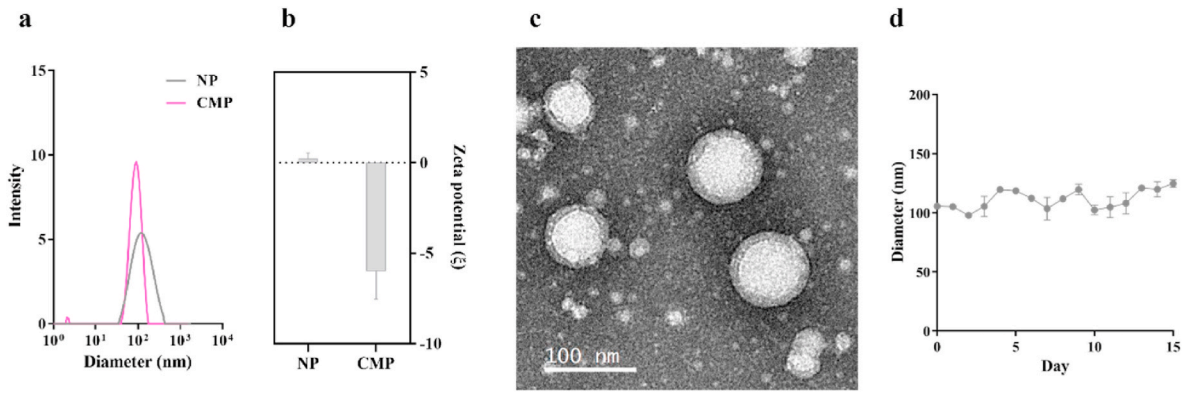

Fig. 1. Characterization of the cell-memetic nanoparticle (CMP) comprising sialic acid inserted in an mPEG-b-PLA nanoparticle. (a) Size distribution and (b) zeta potential of the CMPs and mPEG-b-PLA nanoparticles without sialic acid (NP), measured using dynamic light scattering (DLS). Morphology of the CMP was analyzed by (c) transmittance electron microscopy. (d) Colloidal stability of CMP stored in the refrigerator at 4 °C was monitored for two weeks using DLS. Error bars represent standard deviation; $n = 3$.

mPEG-b-PLA into CMPs. Additionally, the colloidal stability of CMPs was investigated because stable maintenance of the cell-mimicking structure of CMPs was required for the highly selective signal production that mediates viral fusion. We measured the diameter of CMPs stored in the refrigerator at 4 °C for two weeks and found no significant change in diameter from the initial value of approximately 100 nm (Fig. 1(d)).

3.2. Optimization of FRET signal generated by perturbing the membrane structure

To mediate membrane fusion between CMPs and AIV, we first evaluated the ability of CMPs to withstand a biological environment and generate fluorescence signals in response to perturbative stimuli on the membrane structure (Chen et al., 2008). The fluorescence spectrum of CMPs was determined under acidic, basic, and neutral pH conditions, with the maximum emission occurring at 569 nm and excitation at 475 nm. The result can be explained that proximity of Two hydrophobic dyes incorporated in the membrane of CMP induces FRET effect, revealing an enhanced acceptor emission at 569 nm and extinguished donor emission at 504 nm. Even in the presence of enzymes, the FRET effect of the donor and acceptor dyes encapsulated in the CMPs was maintained, indicating that the CMPs were stable in a biological environment (Fig. S2(a)), whereas CMPs treated with 1% Triton X-100, a membrane solubilizer, exhibited the highest fluorescence emission at 504 nm (Fig. S2(b)). This result can be explained by a disruption in the CMP nanostructure caused by Triton X-100, which resulted in a weakened FRET effect between FRET pairs (Xie et al., 2016; Yoon et al., 2006). The destabilization of CMPs by Triton X-100 can be viewed as an extreme condition that generates a FRET-based signal in response to a burst of FRET fluorophores from the disrupted membrane structure. We used the FRET efficiency to characterize the relative changes in energy migration between the donor and acceptor fluorophores for the analysis of FRET-based signals. The FRET efficiency was 0.9, close to 1, for a stable CMP structure in distilled water (DW), as measured by the ratio of the donor's fluorescence intensity to the summation of the donor and acceptor fluorescence. The FRET efficiency of the CMPs remained relatively constant under neutral and acidic conditions, as well as in the presence of enzymes, indicating that CMPs had a stable structure that endured biological environments (Fig. S2(c)) (Kim et al., 2018). In comparison, the FRET efficiency of CMPs treated with Triton X-100 (1%) reached approximately 0.3 in 20 min, indicating that CMPs capable of generating FRET-based signals can direct membrane structure perturbations. To normalize changes in the FRET efficiency of CMPs mediating the exterior stimulus, we arbitrarily implemented FRET efficiency change (FEC) (%), considering that the FRET efficiency of CMPs was minimal (0%) in DW and maximal (100%) in the Triton X-100 (1%) treatment (Fig. S2(d)). Additionally, the introduced FEC (%) may be advantageous in terms of the applicability of the detection platform to fecal samples containing a variety of biological molecules that may affect the measurement of fluorescence intensity. In a biological environment, a normalized FRET-based signal can help reduce the off-target effects.

3.3. Evaluation of the membrane fusion activity of cell-mimetic nanoparticles

To determine the capability of CMP to detect influenza virus via viral fusion, CMP was incubated with LPAIV (H9N2) cultured in eggs and trypsin for 40 min, followed by a 4-h kinetic analysis of FEC (%) under acidic conditions (Fig. 2(a)). Within 20 min, the FEC (%) of CMPs increased significantly under the membrane fusion activity condition (activated H9N2) compared to that at baseline, whereas no change was observed when CMPs were simply mixed with H9N2 (non-activated). However, even after incubation with activated H9N2, polymeric vesicles prepared with mPEG-b-PLA without sialic acid (NP) did not exhibit a significant change in FEC (%) value over time (Fig. 2(b)). This demonstrates that CMPs can successfully probe the fusogenicity of AIV under membrane fusion activity conditions via sialic acid-mediated binding to H9N2. Additionally, the FEC (%) of CMPs was up to six times that of polymer nanoparticles containing no sialic acid (NPs) after 20 min (Fig. 2(c)). The FEC (%) of CMPs reflected an increase in the fluorescence intensity (FI) of the donor and a decrease in that of the FI of the acceptor as compared to the baseline, indicating viral fusion of activated H9N2 (Fig. S3(a)). The NPs, conversely, were unable to probe the fusion activity of activated H9N2, indicating a slightly decreased FI of both the donor and acceptor in comparison to the baseline (Fig. S3(b)**).** By comparing the responses of CMPs and NPs to activated influenza virus, we established that the sialic acid-inserted nanostructure was critical in mediating membrane fusion with the influenza virus. Thus, CMPs are suitable for probing the fusion activity of and ultimately detecting AIV (Fig. 3). As a diagnostic assay, we investigated the dose-response relationship associated with virus exposure levels to provide criteria for the detection limit as well as an in-depth understanding of the detection mechanism. We determined the FEC (%) of CMPs in response to H9N2 (LPAIV) at various viral titers in both non-activated and activated states (Fig. S4). CMP produced a viral titer-dependent signal following a linear regression in the presence of trypsin, whereas CMP did not exhibit a strong dose-response effect in the absence of trypsin. Thus, CMP generated a distinct signal that mediated the fusogenic activity of AIV under precisely controlled activation conditions, which demonstrates its diagnostic potential.

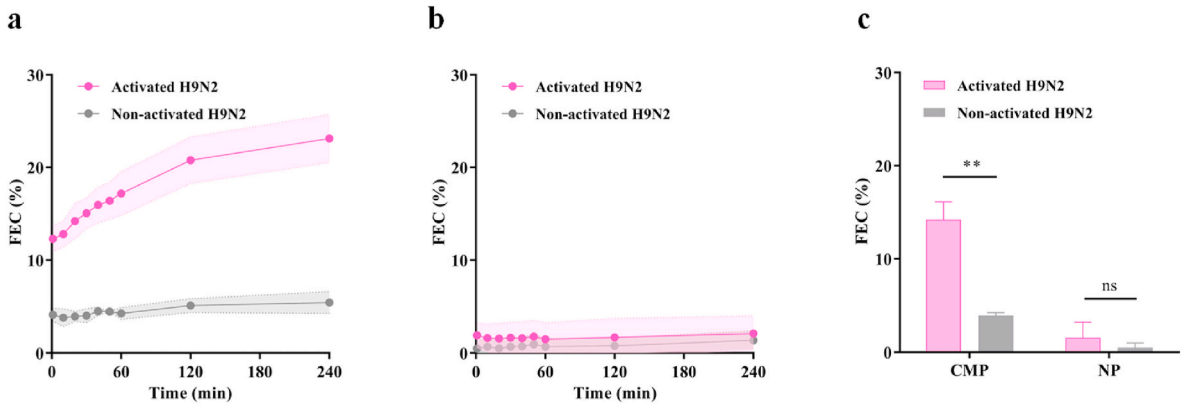

Fig. 2. Evaluation of membrane fusion activity of the cell-mimetic nanoparticle (CMP). Kinetics of FEC (%) from (a) CMP and (b) nanoparticles without sialic acid (NP), treated with H9N2 and trypsin at pH 5.5 (activated H9N2), and only H9N2 at pH 7.4 (non-activated H9N2). (c) FEC (%) analysis of NPs and CMPs in response to activated H9N2 and non-activated H9N2 at 20 min. Color shaded bands represent the uncertainty regions (error bars). Error bars indicate standard deviation with $n = 3$ (**p < 0.01).

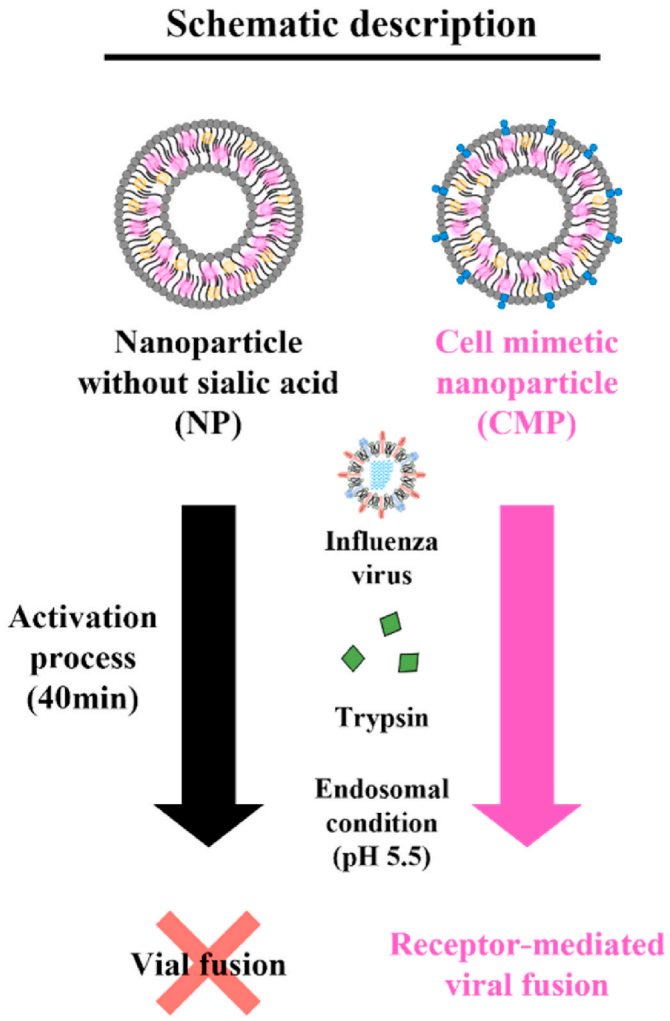

Fig. 3. Schematic description of the CMP-based assay. Infiltration of CMP was enabled by the activation of AIV via sialic acid-mediated viral fusion; membrane fusion induced a FRET signal change driven by structural deformation of CMP.

To further characterize the viral fusion event between CMP and AIV, we used confocal microscopy for imaging analysis. We prepared CMP and H9N2 (LPAIV) labelled with the DiO and DiI fluorophores and analyzed the images of CMP incubated with H9N2 under non-activated and activated conditions (Fig. 4(a)-(b)). Activation resulted in a more coherent distribution profile for CMP and H9N2, compared with that for CMP and non-activated H9N2, implying viral fusion between CMP and activated H9N2. To quantify the colocalization of CMP and H9N2 under these conditions, we determined the fluorescence signal of CMP and H9N2 using ImageJ and calculated colocalization (%) by comparing the intersection area to the sum of the fluorescence signals of the two components (Fig. 4(c)). The colocalization of CMP with H9N2 was significantly higher ($p < 0.01$) when the virus was activated (44%) than when it was not activated (18%). The results indicated that viral fusion of CMP and H9N2 was a distinct phenomenon in comparison to simple receptor-mediated binding that may occur in the absence of infection. Thus, trypsin-induced activation was required for AIV fusion and CMPs facilitated signal production in response to the fusion event. Furthermore, we performed transmission electron microscopy (TEM) analysis and observed the viral fusion event between CMP and activated H9N2, where CMP bound to non-activated H9N2 but did not fuse (Fig. S5).

3.4. Discrimination of HPAIV from LPAIV via disparity in enzymatic activation

When developing diagnostic assays, it is critical to establish valid positive criteria based on the physiological characteristics of the virus to ensure accurate and sensitive detection. Therefore, we investigated differences in the protease-mediated activation levels of AIV, which is a factor in pathogenicity. Detection criteria were established to reflect the enzyme-mediated activation of HPAIV by trypsin and furin, whereas LPAIV is activated exclusively by trypsin in an endosomal environment (Harrison, 2008). To assess the ability of CMPs to identify LPAIV and HPAIV, we determined the FEC (%) of CMPs in response to AIV incubated with trypsin or furin at pH 5.5 and that in response to AIV at pH 7.4 (Fig. 5). We assessed 11 LPAIVs (H1N1, H2N5, H3N1, H4N6, H5N2, H6N8, H7N7, H9N2, H9N10, H10N7, and H11N9) and two HPAIVs (H5N1 and H5N6). We used a two-step process to detect AIVs and characterize their pathogenicity by comparing the enzymatic activation patterns of the LPAIVs and HPAIVs (Fig. S6). First, we determined the FEC (%) of CMPs that responded to a negative set-up and were activated by trypsin, a common enzyme that mediates fusogenic activity of AIVs. In response to LPAIVs, CMP demonstrated significantly greater FEC (%) under trypsin-induced activation conditions than that under inactive and furin-induced activation conditions (Table S1). This is likely due to trypsin-induced cleavage of LPAIVs which activated their fusogenic behavior and fused them with CMPs, exposing the FRET-off signal. However, when HPAIVs were assessed, CMPs showed an increase in FEC

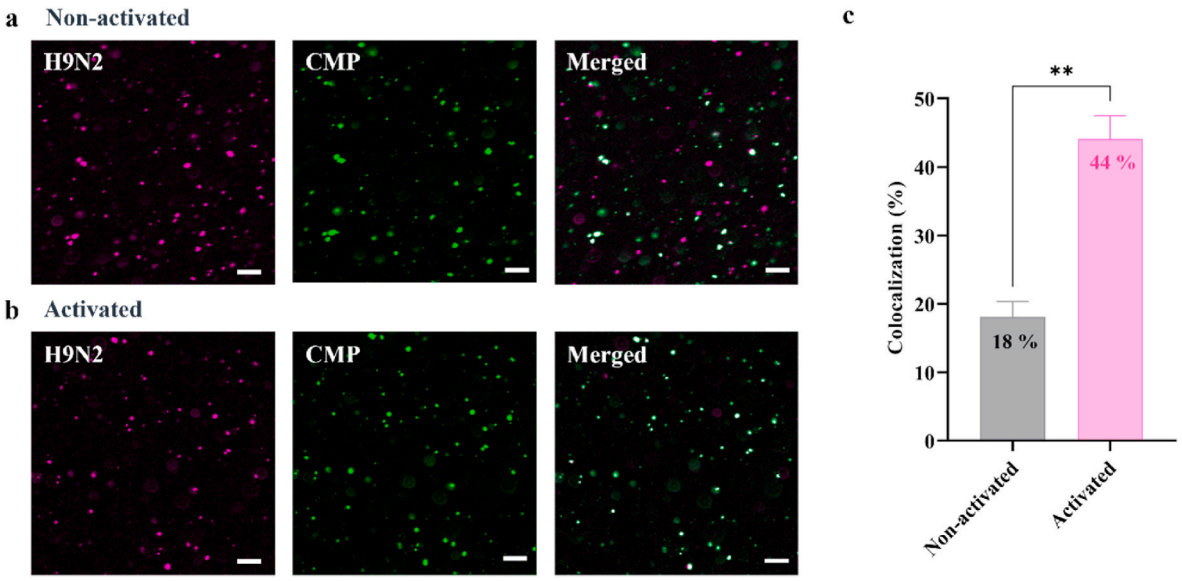

Fig. 4. Colocalization of CMP and H9N2 under non-activated and activated conditions. H9N2 and CMP were stained with fluorophore DiI (magenta) and DiO (green), respectively. Confocal images of (a) CMP with non-activated H9N2 and (b) CMP with activated H9N2 (trypsin-induced). Scale bar = 10 μm. (c) The colocalization (%) of CMP and H9N2 under non-activated and activated conditions were quantified and analyzed. Error bars represent standard deviation with $n = 3$ (**p < 0.01).

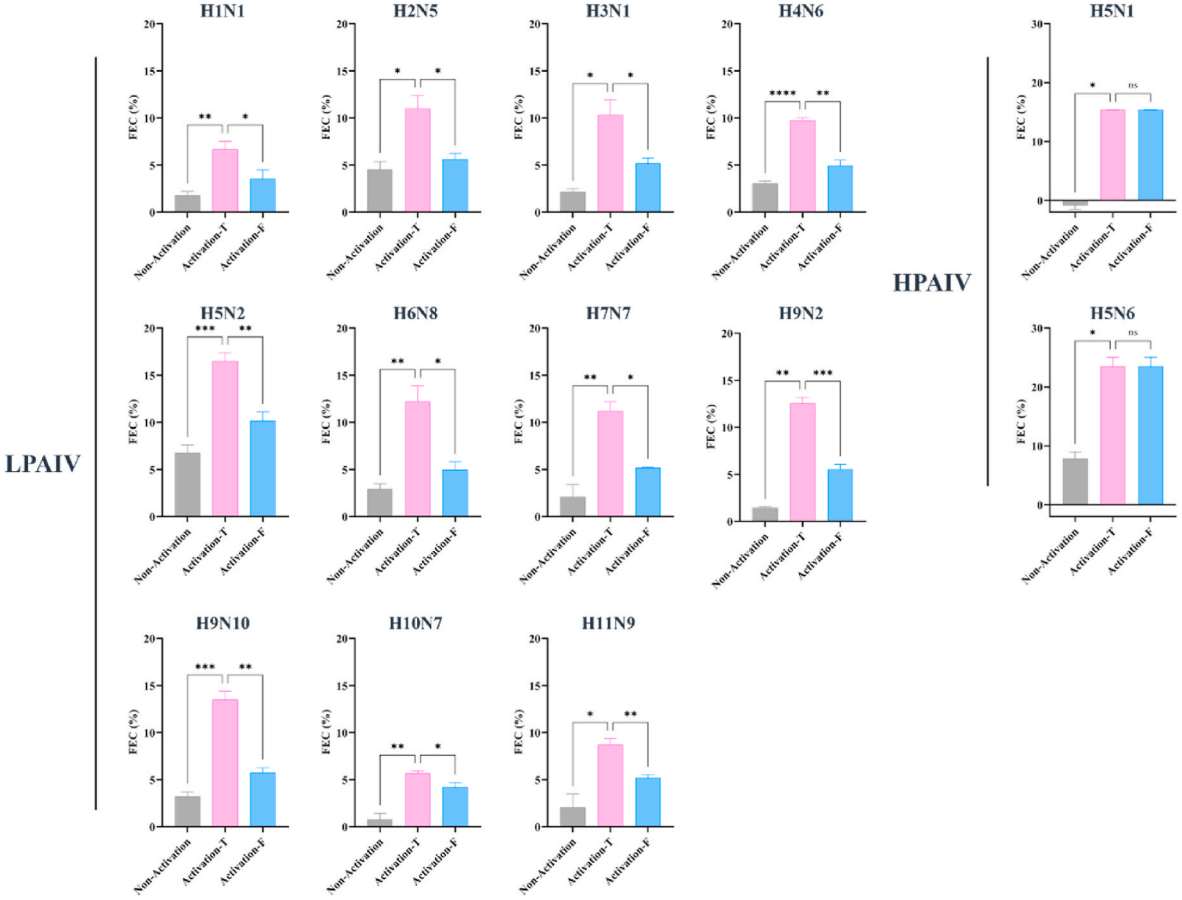

Fig. 5. Evaluation of CMP detection of LPAIV and HPAIV from egg-cultured viral specimens. FRET efficiency change (FEC) (%) of CMP was evaluated with the treatment of pH 7.4 solution (non-activation), trypsin at pH 5.5 (activating condition for both LPAIV and HPAIV; activation-T), and furin at pH 5.5 (activating condition for HPAIV alone; activation-F). Error bars represent standard deviation with $n = 3$ (*p < 0.05, **p < 0.01, ***p < 0.001).

(%) under both enzymatic activation conditions compared with that under the non-activation condition. There was a pathogenicity-dependent difference in the test results under furin-induced activation conditions, indicating that CMP can signal different fusogenic behaviors of HPAIV and LPAIV via disparities in enzymatic activation. The results demonstrated that CMPs specifically detected influenza viruses and discriminated between HPAIV and LPAIV via viral fusion.

3.5. Evaluation of the effectiveness of CMP-based detection in fecal samples

As the detection of avian influenza virus is primarily performed on fecal specimens, the signals generated by diagnostic assays may be influenced by various biomolecules found in feces. Due to the impure nature of fecal samples, conventional diagnostic tools such as rapid kits have low sensitivity, and setting a clear detection threshold is difficult. Thus, we established a strategy for overcoming these sample-related challenges by comparing the FEC (%) values under controlled conditions. To determine the practical applicability of the diagnostic assay, we evaluated its detection performance using fecal samples spiked with various types of AIV. HPAIV-spiked samples were prepared using duck and chicken feces to mimic AIV-infected poultry feces. To determine pathogenicity, we conducted a statistical analysis comparing trypsin-induced activation with furin-induced activation. For LPAIVs, the FEC (%) of CMPs activated by trypsin was significantly greater than that under the other conditions (Table S2). In contrast, CMPs that showed increased FEC (%) under both enzyme-induced conditions compared with that in the non-activated condition identified true-positive HPAIV fecal samples (Fig. 6(a)). The test results revealed pathogenicity-dependent signal production, demonstrating the efficacy of this assay as a diagnostic assay applicable to biological samples. To determine the competitiveness of CMP as a diagnostic tool, we compared its detection performance with that of a commercially available rapid immunoassay kit. CMP successfully detected all HPAIV fecal samples, whereas the rapid kit detected six of eight samples, demonstrating the superior sensitivity of CMP (Fig. 6(b)). In conclusion, CMPs have the advantages of detecting HPAIVs and LPAIVs that rapid kits cannot, as well as increased sensitivity for fecal sample detection (Table S3).

3.6. Cross-reactivity of CMPs

Cross-reactivity can result in false-positive detection results, which is a significant factor that must be adequately analyzed to demonstrate the selectivity and reliability of diagnostic technology. To further investigate the cross-reactivity of the cell-mimetic nanoparticles, we evaluated them against a variety of viruses, including Newcastle disease virus (NDV), porcine epidemic diarrhea virus (PEDV), canine distemper virus (CDV), porcine reproductive and respiratory syndrome virus (PRRSV), and infectious canine hepatitis virus (ICHV) (Fig. S7). The results confirmed the absence of cross-reactivity in the CMPs (Table S4). CMPs generated a detection signal via membrane fusion that mimicked the cell penetration mechanism of AIV and resulted in high specificity for AIV. Additionally, we assessed the sensitivity and specificity of CMP for the diagnosis of HPAIV and LPAIV. We assessed 79 samples (Fig. S8), including 55 LPAIVs and 17 HPAIVs. We determined that 53 of 55 LPAIV-positive samples were true positives, whereas all HPAIV-positive samples were true positives (Table S5). The sensitivity (true positive/total positive) and specificity (true negative/total negative) of the detection of LPAIVs and HPAIVs were calculated. LPAIV detection had a sensitivity of approximately 96.4% and a specificity of 100%, and HPAIV detection had a sensitivity and specificity of 100% each.

4. Conclusions

In this study, we developed cell-mimetic nanoparticles for rapidly detecting HPAIV and LPAIV via viral fusion. CMPs containing sialic acid and FRET dye pairs exhibited FRET off in response to membrane fusion

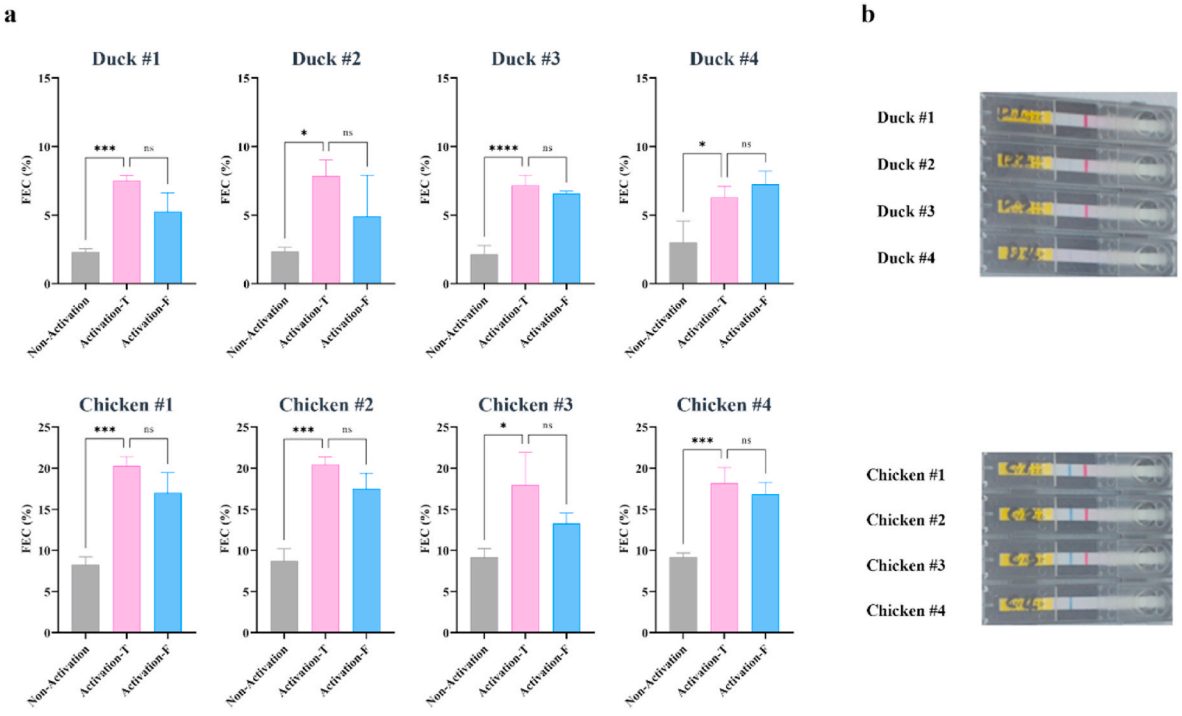

Fig. 6. Comparison between CMP and rapid assay kits in the detection of viruses from fecal samples spiked with the HPAIV H5N6. (a) Two types of feces, including duck and chicken, were used for the preparation of HPAIV fecal samples. Each sample was investigated under three conditions: neutral non-activation, trypsin-induced activation (activation-T), and furin-induced activation (activation-F). Conversely, (b) the rapid kit was conducted under neutral pH. Error bars represent standard deviation with $n = 3$ (*$p < 0.05$, ***$p < 0.001$, ****$p < 0.0001$).

with an activated virus, whereas nanoparticles lacking sialic acid exhibited little response, indicating that AIV was bound via cellular receptors. HPAIV and LPAIV were detected using criteria established by the physiological characteristics of AIV for activating viral fusion, including the endosomal environment and enzyme-specific cleavage disparity (Worch, 2013). We introduced FEC (%) and precisely detected various LPAIVs and HPAIVs in egg-cultured and fecal-spiked specimens by determining the level of the FRET-off effect caused by viral fusion. Using a data processing strategy for fluorescent signals derived from virus tests, we determined the performance of the diagnostic assay for various types of specimens. CMPs not only detected LPAIV and HPAIV but also demonstrated superior sensitivity in comparison to rapid kits that only non-specifically detect AIV. Furthermore, our current approach for probing fusion activity indicates the ability of AIV to infect host cells, which other conventional assays do not reveal. Cross-reactivity testing revealed that the CMP assay for HPAIV and LPAIV detection was specific, satisfying one of the fundamental aspects of diagnostics. Thus, we believe that our system can serve as an effective diagnostic assay to rapidly detect LPAIV and HPAIV, reducing economic losses associated with viral outbreaks through the implementation of preventative measures.

CRediT authorship contribution statement

Geunseon Park: Conceptualization, Writing – original draft, Investigation. **Jong-Woo Lim:** Visualization, Investigation. **Chaewon Park:** Data curation, Validation. **Minjoo Yeom:** Resources, Validation. **Sojeong Lee:** Methodology, Investigation. **Kwang-Soo Lyoo:** Resources. **Daesub Song:** Writing – review & editing. **Seungjoo Haam:** Supervision.

Declaration of competing interest

The authors declare that they have no known competing financial interests or personal relationships that could have appeared to influence the work reported in this paper.

Acknowledgments

This research was supported by grants from the Korea Mouse Phenotyping Project (NRF-2019M3A9D5A01102797) of the Ministry of Science and ICT through the National Research Foundation (NRF). S. Haam acknowledges support from the Korea Environment Industry & Technology Institute (KEITI) through the Technology Development Project for Biological Hazards Management in Indoor Air Project, funded by Korea Ministry of Environment (MOE) (RE202101004). This work was also funded by Bio & Medical Technology Development Program of the National Research Foundation through the Ministry of Science & ICT (NRF-2018M3A9E2022819).

Appendix B. Supplementary data

Supplementary data to this article can be found online at https://doi.org/10.1016/j.bios.2022.114407.

References

Barrabés, S., Sarrats, A., Fort, E., De Llorens, R., Rudd, P.M., Peracaula, R., 2010. Electrophoresis 31 (17), 2903–2912.
Chen, H., Kim, S., Li, L., Wang, S., Park, K., Cheng, J.-X., 2008. Proc. Natl. Acad. Sci. Unit. States Am. 105 (18), 6596–6601.
Chen, Z., Lv, Z., Wang, X., Yang, H., Qing, G., Sun, T., 2018. NPG Asia Mater. 10 (3), e472.
Collins, A., Azmat, F., Rentschler, R., 2019. Stud. High Educ. 44 (8), 1475–1487.
Fukuyama, S., Katsura, H., Zhao, D., Ozawa, M., Ando, T., Shoemaker, J.E., Ishikawa, I., Yamada, S., Neumann, G., Watanabe, S., 2015. Nat. Commun. 6 (1), 1–8.
Galloway, S.E., Reed, M.L., Russell, C.J., Steinhauer, D.A., 2013. PLoS Pathog. 9 (2), e1003151.
Harrison, S.C., 2008. Nat. Struct. Mol. Biol. 15 (7), 690–698.
Hennechart-Collette, C., Martin-Latil, S., Guillier, L., Perelle, S., 2014. J. Appl. Microbiol. 116 (1), 179–190.
Höfle, U., Van de Bildt, M.W., Leijten, L.M., Van Amerongen, G., Verhagen, J.H., Fouchier, R.A., Osterhaus, A.D., Kuiken, T., 2012. Avian Pathol. 41 (6), 547–553.
Imai, M., Watanabe, T., Hatta, M., Das, S.C., Ozawa, M., Shinya, K., Zhong, G., Hanson, A., Katsura, H., Watanabe, S., 2012. Nature 486 (7403), 420–428.
Kim, H.-O., Lim, J.-W., Choi, J., Lee, H., Son, H.Y., Kim, J., Park, G., Chun, H., Song, D., Huh, Y.-M., 2017. J. Mater. Chem. B 5 (48), 9571–9578.
Kim, H.O., Kim, E., An, Y., Choi, J., Jang, E., Choi, E.B., Kukreja, A., Kim, M.H., Kang, B., Kim, D.J., 2013. Macromol. Biosci. 13 (6), 745–754.
Kim, H.O., Na, W., Yeom, M., Choi, J., Kim, J., Lim, J.W., Yun, D., Chun, H., Park, G., Park, C., 2018. Adv. Funct. Mater. 28 (34), 1800960.
Kittel, C., Sereinig, S., Ferko, B., Stasakova, J., Romanova, J., Wolkerstorfer, A., Katinger, H., Egorov, A., 2004. Virology 324 (1), 67–73.
Lee, H., Jin, W., Jeong, B.-C., Suh, J.-W., 2016. Sci. Rep. 6 (1), 1–9.
Lee, P.S., Zhu, X., Yu, W., Wilson, I.A., 2015. J. Virol. 89 (14), 7417–7420.
Manicassamy, B., Manicassamy, S., Belicha-Villanueva, A., Pisanelli, G., Pulendran, B., García-Sastre, A., 2010. Proc. Natl. Acad. Sci. Unit. States Am. 107 (25), 11531–11536.
Neumann, G., Noda, T., Kawaoka, Y., 2009. Nature 459 (7249), 931–939.
Nyan, D.-C., Swinson, K.L., 2015. Sci. Rep. 5 (1), 1–9.
Peterson, A.M., Tan, Z., Kimbrough, E.M., Heemstra, J.M., 2015. Anal. Methods 7 (16), 6877–6882.
Stech, J., Garn, H., Wegmann, M., Wagner, R., Klenk, H., 2005. Nat. Med. 11 (6), 683–689.
Tsang, M.-K., Ye, W., Wang, G., Li, J., Yang, M., Hao, J., 2016. ACS Nano 10 (1), 598–605.
Wagner, R., Gabriel, G., Schlesner, M., Alex, N., Herwig, A., Werner, O., Klenk, H.-D., 2013. Emerg. Microb. Infect. 2 (1), 1–9.
Wang, S., Chen, C., Yang, Z., Chi, X., Zhang, J., Chen, J.-L., 2016. Sci. Rep. 6 (1), 1–12.
Welch, B.D., Yuan, P., Bose, S., Kors, C.A., Lamb, R.A., Jardetzky, T.S., 2013. PLoS Pathog. 9 (8), e1003534.
Worch, R., 2013. FEBS Lett. 587 (18), 2980–2983.
Xiao, R.Z., Zeng, Z.W., Zhou, G.L., Wang, J.J., Li, F.Z., Wang, A.M., 2010. Int. J. Nanomed. 5, 1057.
Xie, M., Wang, S., Singh, A., Cooksey, T.J., Marquez, M.D., Bhattarai, A., Kourentzi, K., Robertson, M.L., 2016. Soft Matter 12 (29), 6196–6205.
Yassine, H.M., Boyington, J.C., McTamney, P.M., Wei, C.-J., Kanekiyo, M., Kong, W.-P., Gallagher, J.R., Wang, L., Zhang, Y., Joyce, M.G., 2015. Nat. Med. 21 (9), 1065–1070.
Ye, W.W., Tsang, M.K., Liu, X., Yang, M., Hao, J., 2014. Small 10 (12), 2390–2397.
Yoon, S.-W., Chen, N., Ducatez, M.F., McBride, R., Barman, S., Fabrizio, T.P., Webster, R. G., Halilloglu, T., Paulson, J.C., Russell, C.J., 2015. Sci. Rep. 5 (1), 1–14.
Yoon, T.-Y., Okumus, B., Zhang, F., Shin, Y.-K., Ha, T., 2006. Proc. Natl. Acad. Sci. Unit. States Am. 103 (52), 19731–19736.
Zhu, Z., 2013. Biomaterials 34 (38), 10238–10248.